Efficient Observer Design for Ambulatory Estimation of Body Centre of Mass Position

Marco Maddalena, *Member, IEEE*, and Mozafar Saadat, *Senior Member, IEEE*

Abstract—**Complementary Linear Filter (CLF) is a common techinque employed for estimating the ground projection of body Centre of Mass starting from ground reaction forces. This method fuses centre of pressure position and double integration of horizontal forces, selecting best cut-off frequencies for low-pass and high-pass filters. Classical Kalman filter is a substantially equivalent approach, as both methods rely on an overall quantification of error/noise and don't analyze its origin and time-dependence. In order to overcome such limitations, a Time-Varying Kalman Filter (TVKF) is proposed in this paper: the effect of unknown variables is directly taken into account by employing a statistical description which is obtained from experimental data. To this end, in this paper we have employed a dataset of 8 walking healthy subjects: beside supplying gait cycles at different speeds, it deals with subjects in age of development and provides a wide range of body sizes, allowing therefore to assess the observers' behaviour under different conditions. The comparison carried out between CLF and TVKF appears to highlight several advantages of the latter method in terms of better average performance and smaller variability. Results presented in this paper suggest that a strategy which incorporates a statistical description of unknown variables and a time-varying structure can yield a more reliable observer. The demonstrated methodology sets a tool that can undergo a broader investigation to be carried out including more subjects and different walking styles.**

Index Terms—**Locomotion, center of mass, ground projection, observer, estimation, ground reaction forces, complementary linear filter, time-varying Kalman filter.**

I. INTRODUCTION

THE evolution of body Centre of Mass (CoM) position throughout locomotion is a major determinant factor to understand and differentiate human gait [1], [2].

Application of markers on individual's body and camera acquisition allow to estimate the position of body segments [3], [4], while inertial parameters are employed to calculate CoM position for any segment and consequently of the whole body. This Geometrical Method (GM) has several drawbacks,

in addition to equipment cost: its accuracy relies on kinematic and inertial parameters precision and particular care is required in the trial preparation, which in turn translates to considerable demand in terms of time and skill.

During experimental trials for human biomechanical analysis, Ground Reaction Forces (GRF) are often acquired. The force measuring interface is commonly floor-installed [5], [6], yet, in order to allow multiple strides GRF acquisition, it can be alternatively installed either on a treadmill [7], [8] or inside instrumented shoes [9], [10], [11]. Double integration (DI) of GRF allows to straightforwardly calculate the displacement of CoM through a single gait cycle with an accuracy comparable to GM [7], [12], [13]; nonetheless, employing DI for calculating absolute position of CoM would be troublesome, as the estimation is heavily influenced by drift due to initial state error and sensor noise.

This limitation can be mitigated by fusing the outcome of DI with the position of the equivalent GRF application point, called Centre of Pressure (CoP): while DI can provide instantaneous rate of change of CoM evolution, CoP supplies a reference to prevent drift phenomenon [9], [11], [14]. Clearly, this strategy allows to enhance the estimation of CoM position only with regards to its horizontal coordinates, which correspond to its projection on the ground (CoMG). Such information, although incomplete, holds considerable interest in the biomechanical analysis field, in particular it allows the study of balance and dynamic stability during locomotion through the concepts of extrapolated centre of mass position and margin of stability [11], [14], [15], [16], with particular application to neurological disorders [10], [17], [18].

DI and CoP fusion is usually carried out by employing a Complementary Linear Filter (CLF): not considering any statistical description for the noise corrupting the signals, the filter is obtained by a simple analysis in the frequency domain [19]. This technique foresees that a low-pass filter is used to process CoP position while DI outcome is high-pass filtered in order to avoid drift. Complementarity is given as the two filters have the same cut-off frequency.

Kalman filter (KF) [20] can be used as an alternative to CLF: errors introduced by DI and CoP are seen as model and measurement additive noises respectively, characterized by a particular variance. This approach results in a stationary (time-invariant) filter which balances model- and measurement-based estimations according to different noise variances.
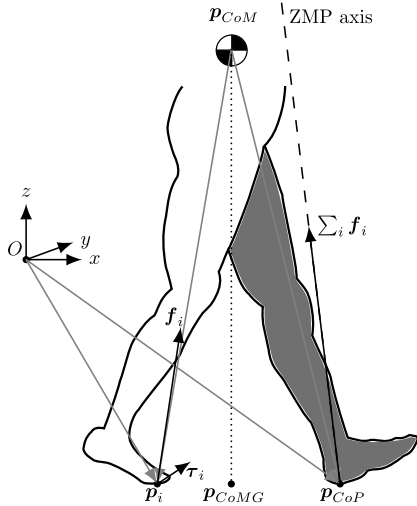
Fig. 1. Forces and moments acting on human body during locomotion and salient points.

It's been proven that CLF and stationary KF are substantially equivalent methods [19], assuming that CLF time constant (corresponding to the chosen cut-off frequency) is set equal to the ratio of standard deviations of measurement and model noises in KF. A legged robot CoM estimation case [21], [22] confirmed that stationary KF is not better than CLF.

Both methods rely on an overall quantification of error/noise and don't analyze its origin and time-dependence. In particular, the goodness of the incorporation of CoP into the estimation is contingent on the hypothesis that angular momentum around CoM is negligible inside the relevant frequency span. Although angular momentum is highly regulated throughout the walking cycle to minimize energy expenditure, substantial segmental momenta do take place (gesticulation), indicating large segment-to-segment cancellations which can cause an important instantaneous variation of whole-body angular momentum [23]. Moreover, the influence of this quantity on estimation is not constant during locomotion, making stationary filters not particularly suitable.

Motivated by these observations, this paper presents a comparison between classical CLF-based observer for CoMG and a novel Time-Varying Kalman Filter (TVKF) which incorporates statistical knowledge of body angular momentum variation in order to refine the estimation.

II. METHODS

A. GRF/CoM Correlation Throughout Locomotion

The combination of forces and moments acting on a human body of mass m during locomotion is summarized in figure 1: force $\boldsymbol{f}_i$ and moment $\boldsymbol{\tau}_i$ operate on a generic body-ground contact point $\boldsymbol{p}_i$, while $\boldsymbol{p}_{CoM}$ indicates the 3d-position of CoM. X-axis is taken in the walking direction, y-axis is transverse while z-axis is vertical. Dynamics yield the equations for the time derivative of linear and angular momentum by summing the effects of forces and moments on all the contact

points, in addition to the gravity acceleration $\boldsymbol{g}$:

$$m\ddot{\boldsymbol{p}}_{CoM} = \sum_i \boldsymbol{f}_i + m\boldsymbol{g} \tag{1a}$$

$$\dot{\boldsymbol{L}} = \sum_i ((\boldsymbol{p}_i - \boldsymbol{p}_{CoM}) \times \boldsymbol{f}_i + \boldsymbol{\tau}_i) \tag{1b}$$

A generic Zero Moment Point (ZMP) $\boldsymbol{p}_{ZMP}$ is defined in such a way that the sum of the moments generated by ground/body contact calculated with respect to that point is null, therefore:

$$\sum_i ((\boldsymbol{p}_i - \boldsymbol{p}_{ZMP}) \times \boldsymbol{f}_i + \boldsymbol{\tau}_i) = \boldsymbol{0} \tag{2}$$

The points which satisfy such definition belong to a straight line in the space (ZMP axis), yet, if ZMP is selected to lie on the ground plane, it can be proven that it corresponds to the CoP position $\boldsymbol{p}_{CoP}$ [24]. Hence, all the points belonging to the ZMP axis can be written as $\boldsymbol{p}_{CoP} + a \sum_i \boldsymbol{f}_i$ for $a \in \mathbb{R}$.

Combining equations 1b and 2, the derivative of the angular momentum turns out to be:

$$\dot{\boldsymbol{L}} = (\boldsymbol{p}_{CoP} - \boldsymbol{p}_{CoM}) \times \sum_i \boldsymbol{f}_i \tag{3}$$

which corresponds to the net moment about the body's CoM. Developing the cross product limited to x- and y-components, the following holds:

$$\begin{cases} \dot{L}^x & = (p_{CoP}^y - p_{CoM}^y)\sum_i f_i^z + p_{CoM}^z \sum_i f_i^y \\ \dot{L}^y & = (-p_{CoP}^x + p_{CoM}^x)\sum_i f_i^z - p_{CoM}^z \sum_i f_i^x \end{cases} \tag{4}$$

Finally, these equations can be re-arranged in order to express the relationship between CoMG and the other elements taken into consideration:

$$\begin{cases} p_{CoM}^x & = p_{CoP}^x + \frac{\sum_i f_i^x}{\sum_i f_i^z} p_{CoM}^z + \frac{\dot{L}^y}{\sum_i f_i^z} \\ p_{CoM}^y & = p_{CoP}^y + \frac{\sum_i f_i^y}{\sum_i f_i^z} p_{CoM}^z - \frac{\dot{L}^x}{\sum_i f_i^z} \end{cases} \tag{5}$$

Force plates measure GRF with good precision, therefore $\sum_i \boldsymbol{f}_i$ and $\boldsymbol{p}_{CoP}$ can be considered as known. Instead, the lack of knowledge of the vertical position of CoM and the derivative of angular momentum due to gesticulation is detrimental to the quantification of CoMG. The variables p_{CoM}^z, $\dot{L}^x$ and $\dot{L}^y$ fluctuate during gait and are periodic with a period corresponding to the stride span, while variation of force sum change the impact of these variables on the difference between CoMG and CoP. In the following sections, two kinds of observers are presented, aiming at estimating p_{CoM}^x and p_{CoM}^y from $\sum_i \boldsymbol{f}_i$ and $\boldsymbol{p}_{CoP}$ while attenuating the effects of unknown variables.

B. Complementary Linear Filter (CLF)

The following development deals with the estimation of x-component of CoM, while the corresponding value for y-component can be found in an equivalent way.

Analysing the two elements of CLF separately, CoP and DI methods for CoM position estimation raise the errors ε_{CoP}^x

and ε_{DI}^x, respectively:

$$\varepsilon_{CoP}^x = p_{CoP}^x - p_{CoM}^x \tag{6a}$$

$$\varepsilon_{DI}^x = \iint \frac{\sum_i f_i^x}{m} \, dt - p_{CoM}^x \tag{6b}$$

X-component of equation 5 shows that ε_{CoP}^x is composed of signals mostly periodical with periods multiple of gait cycle. Therefore, CoP should be processed by a low-pass filter which eliminates the error exceeding a suitable cutoff frequency $\omega_{c,x}$, smaller than step frequency. As proposed by Carpentier et al. [21], a double pole is taken in order to increase the rate of roll-off of the filter:

$$H_{LP,x}(s) = \frac{1}{(1 + \tau_{c,x}s)^2} \tag{7}$$

where time constant $\tau_{c,x} = 1/\omega_{c,x}$. As for DI, a high-pass filter can eliminate drift which is error at zero frequency. This filter is taken as complementary to the low-pass filter, so as to have the same cut-off frequency:

$$H_{HP,x}(s) = 1 - H_{LP,x}(s) = \frac{2\tau_{c,x}s + \tau_{c,x}^2 s^2}{1 + 2\tau_{c,x}s + \tau_{c,x}^2 s^2} \tag{8}$$

Therefore, in the s-domain of Laplace transform, the filter can be written as:

$$\hat{P}_{CoM}^x(s) = H_{LP,x}(s) P_{CoP}^x(s) + H_{HP,x}(s) \frac{1}{s^2} \frac{F^x(s)}{m} \tag{9}$$

Cut-off frequency should be chosen in such a way to minimize estimation error. Filters allow useful signal passing but also error signal in their respective frequency range. Approximating the two filters gain beyond cut-off frequency to zero, we have the following cumulative error power spectral distributions:

$$J_{\varepsilon,CoP}^x(\omega_{c,x}) = \int_0^{\omega_{c,x}} |E_{CoP}^x(j\omega)|^2 \, d\omega \tag{10a}$$

$$J_{\varepsilon,DI}^x(\omega_{c,x}) = \int_{\omega_{c,x}}^{\infty} |E_{DI}^x(j\omega)|^2 \, d\omega \tag{10b}$$

where $E_{CoP}^x(j\omega)$ and $E_{DI}^x(j\omega)$ are Fourier transforms of ε_{CoP}^x and ε_{DI}^x, respectively. Finally, $\omega_{c,x}$ can be taken in order to minimize the total error:

$$\min_{\omega_{c,x}} J_{\varepsilon,CoP}^x(\omega_{c,x}) + J_{\varepsilon,DI}^x(\omega_{c,x}) \tag{11}$$

C. Time-Varying Kalman Filter (TVKF)

Re-writing x-component of equation 5 in a state-space form, we have:

$$\begin{cases} \dot{\boldsymbol{x}} = A\boldsymbol{x} + B(u + \tilde{u}) \\ y = C\boldsymbol{x} + \tilde{v} \end{cases} \tag{12}$$

where the state, the output and the input are defined as:

$$\boldsymbol{x} = \begin{bmatrix} p_{CoM}^x \\ \dot{p}_{CoM}^x \end{bmatrix}, \quad y = p_{CoP}^x, \quad u = \frac{\sum_i f_i^x}{m} \tag{13}$$

and the matrices are:

$$A = \begin{bmatrix} 0 & 1 \\ 0 & 0 \end{bmatrix}, \quad B = \begin{bmatrix} 0 \\ 1 \end{bmatrix}, \quad C = \begin{bmatrix} 1 & 0 \end{bmatrix} \tag{14}$$

The additive signal $\tilde{u}$ is the input uncertainty due to force measure noise, which can be seen as the main contributor to DI drift. It is assumed to be a white Gaussian process with variance $\sigma_{\tilde{u}}^2$. The additive signal $\tilde{v}$, instead, is the output uncertainty:

$$\tilde{v} = -\frac{\sum_i f_i^x}{\sum_i f_i^z} p_{CoM}^z - \frac{\dot{L}^y}{\sum_i f_i^z} \tag{15}$$

The unknown p_{CoM}^z and $\dot{L}^y$ are assumed to be white Gaussian noises as well, so that $p_{CoM}^z \sim \mathcal{N}(\mu_z, \sigma_z^2)$ and $\dot{L}^y \sim \mathcal{N}(0, \sigma_{L,y}^2)$. This can be justified as CoM vertical position oscillates throughout the gait cycle around an average value, while time integral of $\dot{\boldsymbol{L}}$ over a gait cycle is zero as the angular momentum goes back to its initial value. Moreover, it is assumed, by simplicity, that p_{CoM}^z and $\dot{L}^y$ are mutually independent. With this definition, $\tilde{v}$ turns out to be a noise characterized by time-varying stochastic properties.

Hereafter the TVKF development proceeds as a discrete-time system. We assume sample time Δt is sufficiently small so that, at k-th instant t_k, $u(t) \approx u(t_k)$ and $\tilde{u}(t) \approx \tilde{u}(t_k)$ when $t \in [t_k \ t_k + \Delta t]$. The discretized version of the system in equation 12 is therefore:

$$\begin{cases} \boldsymbol{x}_k = A_d \boldsymbol{x}_{k-1} + B_d u_{k-1} + \boldsymbol{w}_k \\ y_k = C_d \boldsymbol{x}_k + v_k + \bar{v}_k \end{cases} \tag{16}$$

where the matrices are defined as:

$$A_d = \begin{bmatrix} 1 & \Delta t \\ 0 & 1 \end{bmatrix}, \quad B_d = \begin{bmatrix} \frac{1}{2}\Delta t^2 \\ \Delta t \end{bmatrix}, \quad C_d = \begin{bmatrix} 1 & 0 \end{bmatrix} \tag{17}$$

Noise $\boldsymbol{w}_k$ accounts for the input uncertainties and its covariance matrix is equal to $Q = \sigma_{\tilde{u}}^2 B_d B_d^T$. Re-arranging the measurement noise of the system in equation 12, the noise signal can be described as $v_k \sim \mathcal{N}(0, r_k^x)$, whose variance is given by:

$$r_k^x = \frac{\left(\sum_i f_i^x\right)^2 \sigma_z^2 + \sigma_{L,y}^2}{\left(\sum_i f_i^z\right)^2} \tag{18}$$

The variable $\bar{v}_k$, instead, is at any instant a determined value equal to $-\frac{\sum_i f_i^x}{\sum_i f_i^z} \mu_z$.

The matrices relating to the TVKF can be subsequently calculated [20], starting from a priori error covariance, Kalman filter gain and update of the a posteriori error covariance matrix:

$$\begin{cases} P_{k|k-1} = A_d P_{k-1} A_d^T + Q \\ K_k = P_{k|k-1} C_d^T \left(C_d P_{k|k-1} C_d^T + r_k^x\right)^{-1} \\ P_k = (I - K_k C_d) P_{k|k-1} \end{cases} \tag{19}$$

so that the state observer can be written as:

$$\begin{aligned} \hat{\boldsymbol{x}}_k = {}& A_d \hat{\boldsymbol{x}}_{k-1} + B_d u_{k-1} \\ & + K_k \left(y_k - \bar{v}_k - C_d(A_d \hat{\boldsymbol{x}}_{k-1} + B_d u_{k-1})\right) \end{aligned} \tag{20}$$

The quantity $y_k - \bar{v}_k$ is the x-axis projection of a particular point $\boldsymbol{p}_{ZMP}^*$ belonging to ZMP axis whose z-component is μ_z (see figure 2):

$$\boldsymbol{p}_{ZMP}^* = \boldsymbol{p}_{COP} + \frac{\mu_z}{\sum_i f_i^z} \sum_i \boldsymbol{f}_i \tag{21}$$
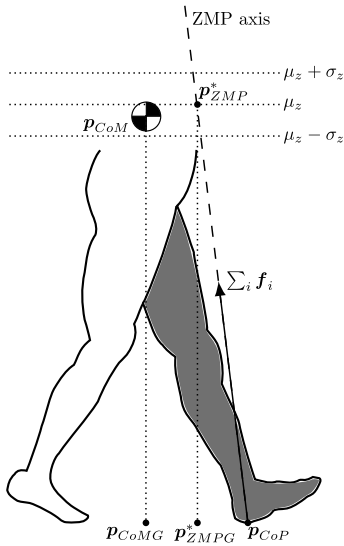
Fig. 2. Salient points for TVKF.

Such projection p_{ZMP}^{*x} can be seen as a first attempt at estimating p_{CoM}^x by refining the rough approximation made by using simply p_{CoP}^x. As a matter of fact, if p_{CoM}^z and $\dot{L}^y$ were known with probability 1, they would coincide with their averages μ_z and 0 respectively, and equation 5 would yield $p_{ZMP}^{*x} = p_{CoM}^x$. Since the variances σ_z^2 and $\sigma_{L,y}^2$ are non-zero, an uncertainty around p_{ZMP}^{*x} is introduced which is described by value r_k^x. As dynamic model uncertainty is given by matrix Q, TVKF gain K_k provides for fusing the two separate estimations according to the different uncertainty levels.

Two different situations are noteworthy. When $|\sum_i f_i^x|$ is maximal, usually at early and late stance phase of gait cycle, distance between p_{ZMP}^x and p_{CoP}^x is also maximal: this means that p_{CoP}^x would be a rather imprecise estimation by itself. At the same time, CoM vertical position variance σ_z^2 has highest influence on r_k^x. Instead, when $\sum_i f_i^x \approx 0$, usually at mid-stance phase of gait cycle, p_{ZMP}^{*x} and p_{CoP}^x coincide and r_k^x is influenced by $\sigma_{L,y}^2$ only.

TVKF development and observations are totally analogous when considering y-component, where for calculating gain we have specific matrix Q, while equation 18 becomes:

$$r_k^y = \frac{(\sum_i f_i^y)^2 \sigma_z^2 + \sigma_{L,x}^2}{(\sum_i f_i^z)^2} \qquad (22)$$

and $\bar{v}_k$ is equal to $-\frac{\sum_i f_i^y}{\sum_i f_i^z}\mu_z$.

D. Experimental Data and Observer Simulation

Real gait data is needed to find proper values for the observer parameters and to provide a comparison in terms of performance, and it would be ideal to make use of data from several subjects walking at different speeds in order to create a complete analysis.

In this paper we have employed a dataset of walking healthy subjects made available at [25] (see table I for sub-

TABLE I
SUBJECTS DESCRIPTION

Subjects number	Gender (F:M)	Age (years)	Mass (Kg)	Leg length (m)
8	6:2	12.9 (3.3)	51.8 (19.2)	0.81 (0.09)

jects' data, [26] and [27] for details about methodology): the participants were given general instructions to walk straight at different speeds during a single testing session. Motion data was collected using a 12-camera Vicon MX system (Vicon, Oxford, UK) operating at 120 Hz, while GRF were recorded using four force plates (AMTI, Watertown, MA), sampled at 1080 Hz. Beside supplying gait cycles at different speeds, the dataset deals with subjects in age of development and provides a wide range of body sizes, allowing therefore to assess the observers' behaviour under different conditions. We have extracted the evolution of GRF (force sum and CoP) and CoM along a single gait cycle for all the 8 subjects at "slow" and "free" speeds and we have utilized MATLAB software (r2021a, the MathWorks Inc., Natick, MA, USA) for processing the data, identifying the filter parameters and calculating the estimation output.

1) Observer Parameters: For the CLF parameters, errors ε_{CoP}^x and ε_{DI}^x are sampled using the extracted data across all subjects and speeds, and their spectral distributions $E_{CoP}^x(j\omega)$ and $E_{DI}^x(j\omega)$ are found through Fast Fourier Transform. Afterwards, the value of $\omega_{c,x}$ is chosen to minimize the sum of cumulative error spectral powers $J_{\varepsilon,CoP}^x(\omega_{c,x})$ and $J_{\varepsilon,DI}^x(\omega_{c,x})$. The procedure is repeated for y-component and $\omega_{c,y}$ is obtained.

For TVKF, the same data is employed to find the stochastic description of force x-component measurement noise in equation 16. Dynamic model error, sampled as $\boldsymbol{w}_k = \boldsymbol{x}_k - A_d\boldsymbol{x}_{k-1} - B_d u_{k-1}$, is used together with the mean $\bar{\boldsymbol{w}}$ to obtain the sample covariance matrix:

$$Q = \frac{\sum_{k=1}^N (\boldsymbol{w}_k - \bar{\boldsymbol{w}})^T(\boldsymbol{w}_k - \bar{\boldsymbol{w}})}{N-1} \qquad (23)$$

Covariance matrix pertaining to force y-component measurement noise is found in the same way. For any subject/speed configuration the following sample mean and variances are found separately:

$$\begin{cases} \hat{\mu}_z = \frac{\sum_{k=1}^N p_{CoM}^z(k)}{N} \\ \hat{\sigma}_z^2 = \frac{\sum_{k=1}^N (p_{CoM}^z(k)-\hat{\mu}_z)^2}{N-1} \\ \hat{\sigma}_{L,x}^2 = \frac{\sum_{k=1}^N M_x^2(k)}{N-1} \\ \hat{\sigma}_{L,y}^2 = \frac{\sum_{k=1}^N M_y^2(k)}{N-1} \end{cases} \qquad (24)$$

where M_x and M_y are x- and y-components of right side of equation 3 (net moment of contact forces around CoM). As these values vary according to subject and speed, it is assumed that they roughly depend on body size, in particular

a first-order polynomial approximation is proposed:

$$\begin{cases} \mu_z = a_1\sqrt{L_{leg}} + b_1 \\ \sigma_z = a_2\sqrt{L_{leg}} + b_2 \\ \sigma_{L,x}^2 = a_3 m L_{leg} + b_3 \\ \sigma_{L,y}^2 = a_4 m L_{leg} + b_4 \end{cases} \qquad (25)$$

where L_{leg} is the subject's leg length, while a_i and b_i least-square fitting from sample values in equation 24.

2) Observer Simulation and Performance: For any subject and speed taken in consideration, the gait cycle data is repeated 20 times to provide force sum, CoP and CoM evolutions which are employed as input and ground truth for the observers. Obviously, the components p_{CoM}^x and p_{CoP}^x are repeated incrementing time by time the reached position.

CLF is simulated on the x-component by defining the filter with the chosen $\omega_{c,x}$ and discretizing it. The obtained difference equation is initialized as the first two values of filter output are set equal to real p_{CoM}^x value plus a random number uniformly distributed in the interval $[-0.2\ 0.2]$ (unit of measure is meter). Y-component is simulated in the same way.

For TVKF simulation, subject's body parameters are firstly used as input for obtaining stochastic parameters through equation 25. Then, estimation is initialized to zero both in position and speed. At any instant k equation 18 yields r_k^x (22 for r_k^y) and matrices in equation 19 are calculated, obtaining the estimation from equation 20.

For performance comparison, the difference between the estimation and the real value of CoMG is taken into consideration at the end of the transient phase. Therefore, for both observers the root mean square error (RMSE) is calculated in the N instants of the interval I corresponding to the 10-th gait cycle. For x-component we have:

$$\text{RMSEx} = \sqrt{\frac{\sum_{k \in I}(p_{CoM}^x(k) - \hat{p}_{CoM}^x(k))^2}{N}} \qquad (26)$$

and analogously for y-component (RMSEy).

III. RESULTS

A. Observer Parameters Identification

Error frequency-domain analysis for CLF parameters identification is displayed in figure 3. Error power spectral density highlights larger low-frequency error for DI-based estimation and larger high-frequency error for CoP-based estimation in both directions, as expected. In particular, CoP-based estimation shows two peaks at frequencies corresponding to "slow" and "free" speed (figures 3A and 3C): for x-component the peaks take place at step frequency (half gait cycle period) and for y-component at stride frequency (whole gait cycle period). The sum of error power spectral distributions shows an area where the minimum value can be picked, between low frequencies and step/stride frequency (figures 3B and 3D). Cut-off frequency ω_c^x is taken equal to 4 [rad/s] while ω_c^y is chosen as 3 [rad/s].

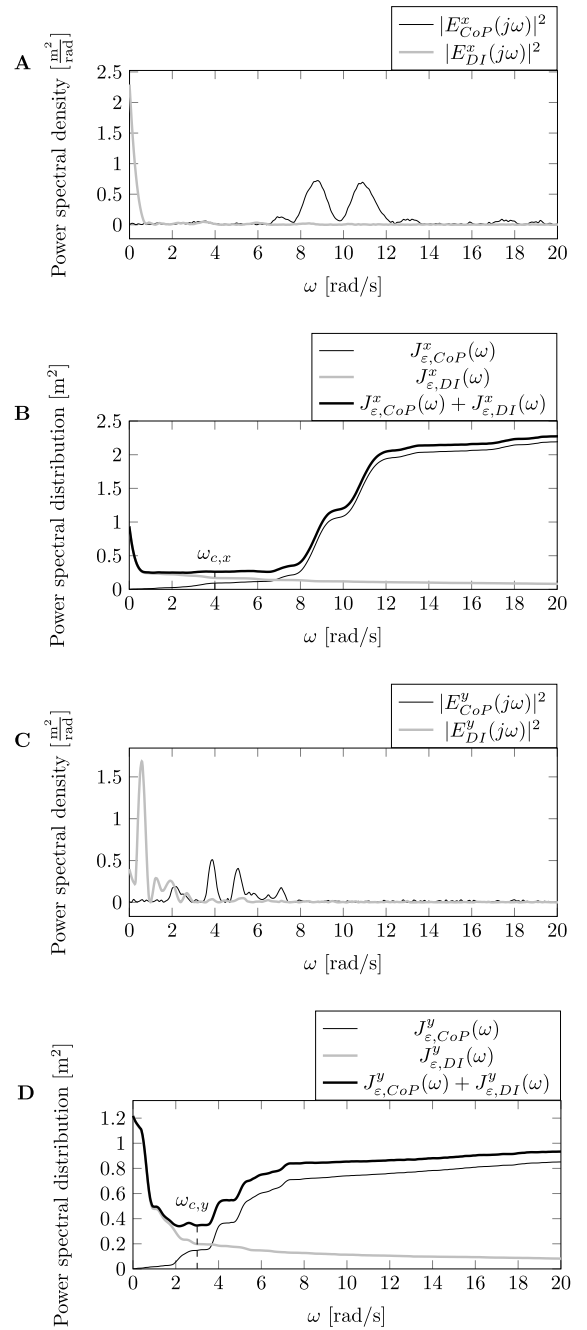Figure 4 shows sample values and linear fitting for identification of TVKF parameters. It can be observed that fitted

Fig. 3. CLF parameters identification. Power spectral density (**A**) and distribution (**B**) of x-component errors. Power spectral density (**C**) and distribution (**D**) of y-component errors.

line predicts mean CoM vertical position rather precisely, while in the other three cases the linear approximation is less definite. Even for the same subject the two sample values can differ considerably when they are acquired at different speeds. In three out of four cases the fitted lines display a positive slope, while standard deviation of CoM vertical position σ_z decreases with square root of leg length. This might seem counter-intuitive, as one could expect the oscillation of CoM to grow, just like the average value does. Yet, as trials have pointed out [28], displacement of CoM throughout locomotion tends to decrease with age due to neural maturation, which
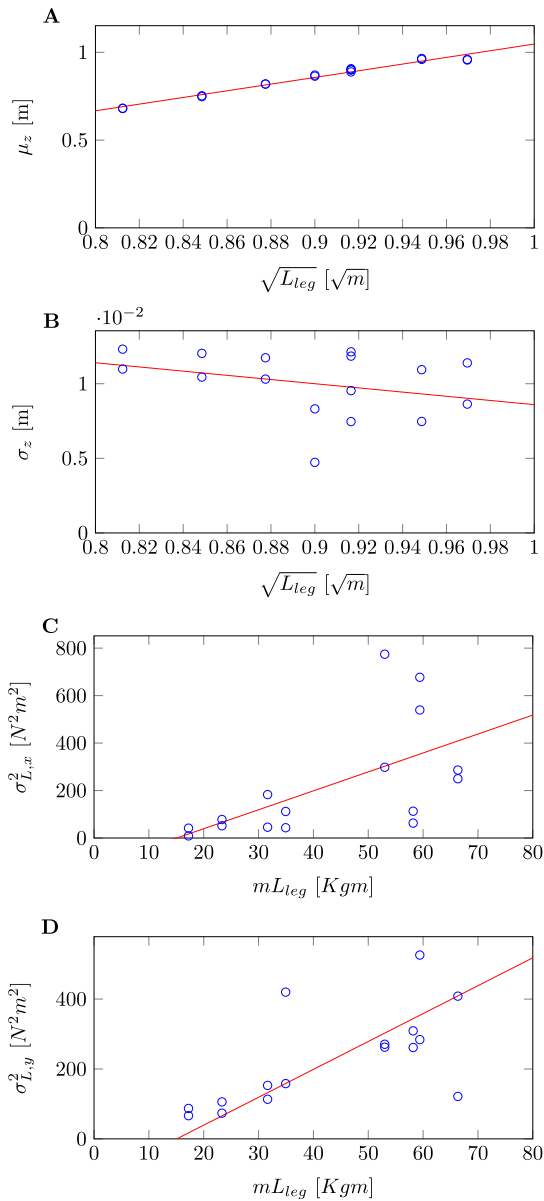
Fig. 4. TVKF parameters identification. Blue circles indicate sample values for any subject/speed configuration, red lines indicate linear fitting. **A**: CoM z-component average μ_z. **B**: CoM z-component standard deviation σ_z. **C**: angular momentum x-component variance $\sigma^2_{L,x}$. **D**: angular momentum y-component variance $\sigma^2_{L,y}$.

TABLE II
PERFORMANCE OF OBSERVERS

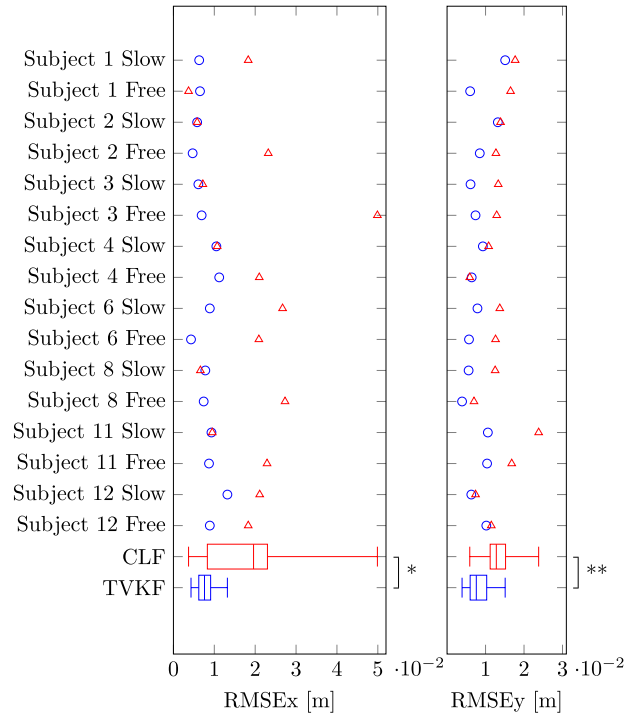| Error	Observer	Quartiles					p-value
		min	25%	median	75%	max	
RMSEx [m]	CLF	0.0043	0.0062	0.0076	0.0091	0.0132	$p < 0.01$
	TVKF	0.0037	0.0083	0.0196	0.0230	0.0499	
RMSEy [m]	CLF	0.0039	0.0060	0.0078	0.0103	0.0151	$p < 0.001$
	TVKF	0.0059	0.0112	0.0128	0.0152	0.0238	

Fig. 5. Comparison of observers performance on x- and y-component: triangles indicate RMSE for CLF and circles for TVKF. In the bottom, box and whisker plots show quartiles distribution of the two observers. Significance of comparison amounts to *$p < 0.01$ and **$p < 0.001$.

means that, when dealing with subjects in the age of development, it is not surprising that a taller individual, which happens to be also older, could show a smaller vertical oscillation.

B. Comparison of Observers

Performance of CLF- and TVKF-based observers in terms of RMSE is reported in table II with quartiles and significance p-value of inter-observer comparison.

Results are presented also graphically in figure 5, where box and whisker plot is added in order to show quartile distribution of the two methods. Values highlight that TVKF has lower average RMSE in both components, with a more remarkable difference for x-component. MATLAB software

has been employed to perform a paired t-test to evaluate significance of RMSE comparison, resulting in p-values $p < 0.01$ for x-component and $p < 0.001$ for y-component. Moreover, CLF features a significantly higher variability, as in several cases it performs just as good as TVKF, while it may show large RMSE up to 5 cm. It is noteworthy that CLF outcome for the same subject may differ depending on the speed; also, for the same subject/speed configuration x- and y-component can show significantly different effectiveness.

This inconstancy in performance is detailed in figures 6 and 7 which provide graphical rendering of data pertaining to subject 1 walking at slow and free speed. They show the evolution through the 10-th gait cycle with regards to x- and y-component of CoM, CoP and estimations (A and B). Also estimation errors in the first 10 seconds are shown (C and D). At slow speed x-component displays a considerable difference between the two observers, while along y-component they are almost identical. At free speed, conversely, x-component behaviour features a strong similarity between the two methods
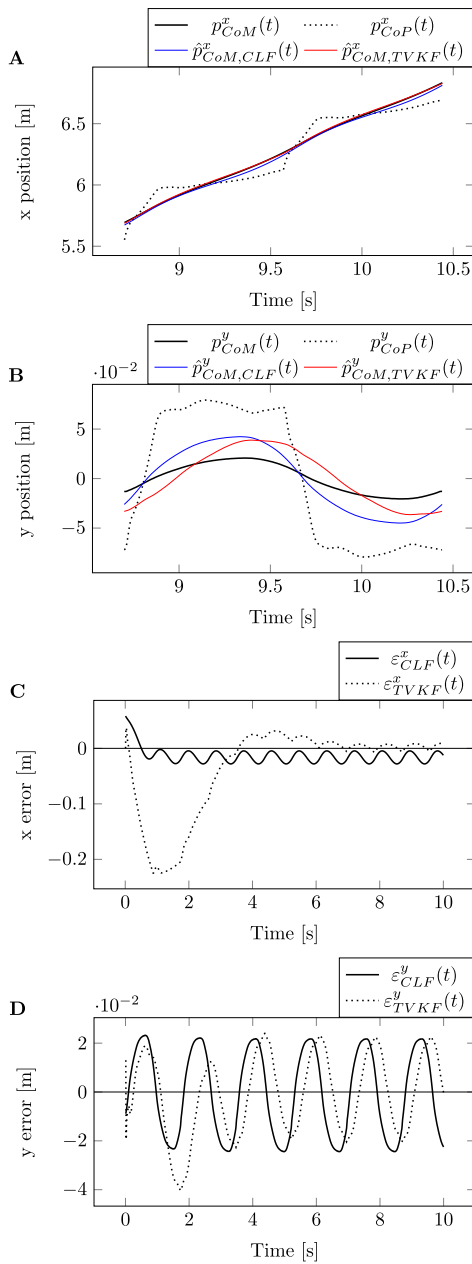
Fig. 6. Observers comaprison for subject 1 at "slow" speed. **A**: x-component of CoM, CoP and CoM estimations. **B**: y-component of CoM, CoP and CoM estimations. **C**: x-component estimation error. **D**: y-component estimation error.
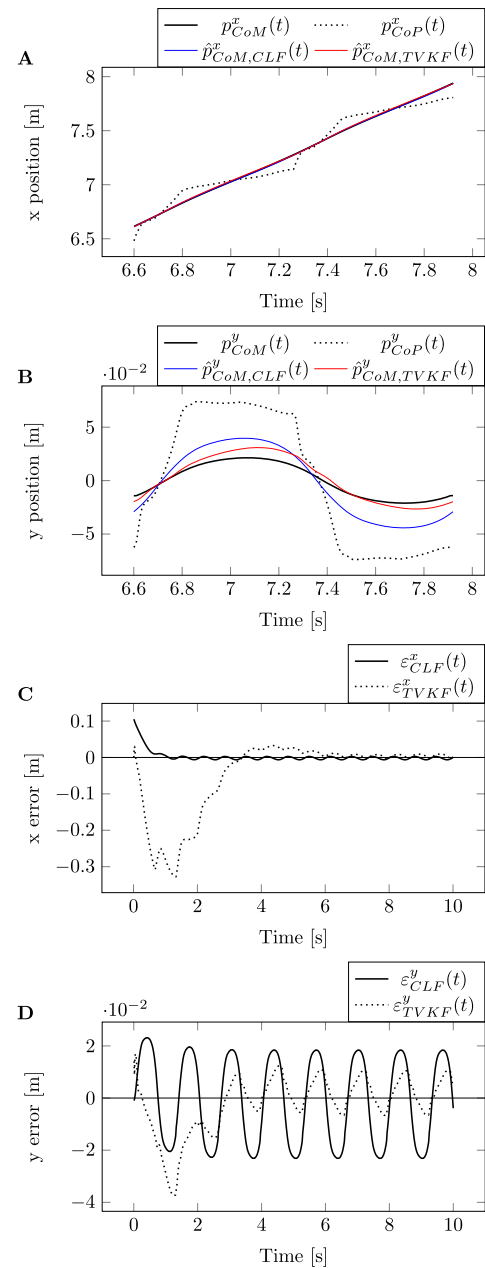

Fig. 7. Observers comaprison for subject 1 at "free" speed. **A**: x-component of CoM, CoP and CoM estimations. **B**: y-component of CoM, CoP and CoM estimations. **C**: x-component estimation error. **D**: y-component estimation error.

and y-component results highlight a better performance by TVKF.

IV. DISCUSSION

The comparison carried out between CLF and TVKF appears to highlight several advantages of the latter method in terms of better average performance and smaller variability. Statistical significance of the comparison confirms that TVKF can be considered a more reliable tool.

CLF can achieve satisfactory estimation error but seems susceptible to walking pattern alteration. This might be partially due to neglecting the effect of variation $\dot{L}$ of angular momentum around the center of mass: in fact, the method

relies on $\dot{L}$ being sufficiently small, or anyway its impact is expected to be described by the error frequency analysis and therefore attenuated through filtering. However, results suggest that even the choice of suitable cut-off frequency is not sufficient to ensure a good performance in any presented condition.

In the development of TVKF, instead, the effect of $\dot{L}$ is directly taken into account by employing a statistical description which is obtained from experimental data. On-line measurement of GRF is exploited to update gain matrix at any instant, therefore making the observer fit to the particular conditions of any phase of gait cycle. This method relies on several assumed simplifications on random variables descrip-

tion, however these don't seem to prevent the observer from estimating CoMG with bounded RMSE in any analyzed case.

The developed strategy allows TVKF to overcome the limitations featured by "classical" KF which foresees a time-invariant structure. For example, KF developed in [22] is based on a discrete-time dynamical model similar to the one expressed by equation 16; however, measurement noise variances are assumed as constant over time and are taken in a rather arbitrary fashion, without incorporation of experimental data, resulting in performance equal to or worse than CLF.

When analyzing the CLF versus TVKF comparison results presented in this paper, however, it should be acknowledged that the range of involved subjects and speeds is rather limited. The comparison could be extended to a larger sample of configurations and walking patterns in order to verify TVKF performance and weigh it against CLF method. Moreover, the additional amount of data would allow to better understand the relations between subject's and TVKF parameters: for example, age could be included as an independent variable to build a more reliable fitting for CoM z-component standard deviation. Generally, a more detailed work could be carried out to achieve a more precise regression of the parameters starting from basic subject's features.

V. CONCLUSION

CLF is commonly considered a valid tool for estimating ground projection of CoM; nonetheless, neglected gait dynamics-related variables can have a significant impact on estimation error. Results presented in this paper suggest that a strategy which incorporates a statistical description of such variables and a time-varying structure can yield a more reliable observer. Indeed, experimental data has been employed to identify TVKF parameters and to compare the performance. The demonstrated methodology sets a tool that can undergo a broader investigation to be carried out including more subjects and different walking styles.

REFERENCES

[1] J. Carpentier, M. Benallegue, and J.-P. Laumond, "On the centre of mass motion in human walking," *Int. J. Autom. Comput.*, vol. 14, no. 5, pp. 542–551, Oct. 2017.

[2] L. Tesio and V. Rota, "The motion of body center of mass during walking: A review oriented to clinical applications," *Frontiers Neurol.*, vol. 10, p. 999, Sep. 2019.

[3] A. G. Kirk, J. F. O'Brien, and D. A. Forsyth, "Skeletal parameter estimation from optical motion capture data," in *Proc. IEEE Comput. Soc. Conf. Comput. Vis. Pattern Recognit.*, vol. 2, Jun. 2005, pp. 782–788.

[4] A. Rastegarpanah and M. Saadat, "Lower limb rehabilitation using patient data," *Appl. Bionics Biomech.*, vol. 2016, pp. 1–10, Sep. 2016.

[5] R. Cross, "Standing, walking, running, and jumping on a force plate," *Amer. J. Phys.*, vol. 67, no. 4, pp. 304–309, Apr. 1999.

[6] C. Lansade, X. Bonnet, N. Marvisi, J. Facione, C. Villa, and H. Pillet, "Estimation of the body center of mass velocity during gait of people with transfemoral amputation from force plate data integration," *Clin. Biomech.*, vol. 88, Aug. 2021, Art. no. 105423.

[7] G. Pavei, E. Seminati, D. Cazzola, and A. E. Minetti, "On the estimation accuracy of the 3D body center of mass trajectory during human locomotion: Inverse vs. forward dynamics," *Frontiers Physiol.*, vol. 8, p. 129, Mar. 2017.

[8] E. M. Day, R. S. Alcantara, M. A. McGeehan, A. M. Grabowski, and M. E. Hahn, "Low-pass filter cutoff frequency affects sacral-mounted inertial measurement unit estimations of peak vertical ground reaction force and contact time during treadmill running," *J. Biomech.*, vol. 119, Apr. 2021, Art. no. 110323.

[9] H. M. Schepers, E. H. F. V. Asseldonk, J. H. Buurke, and P. H. Veltink, "Ambulatory estimation of center of mass displacement during walking," *IEEE Trans. Biomed. Eng.*, vol. 56, no. 4, pp. 1189–1195, Apr. 2009.

[10] F. B. Van Meulen, D. Weenk, J. H. Buurke, B.-J.-F. Van Beijnum, and P. H. Veltink, "Ambulatory assessment of walking balance after stroke using instrumented shoes," *J. NeuroEng. Rehabil.*, vol. 13, no. 1, pp. 1–10, Dec. 2016.

[11] M. I. M. Refai, B.-J.-F. Van Beijnum, J. H. Buurke, and P. H. Veltink, "Gait and dynamic balance sensing using wearable foot sensors," *IEEE Trans. Neural Syst. Rehabil. Eng.*, vol. 27, no. 2, pp. 218–227, Feb. 2019.

[12] M. H. A. Eames, A. Cosgrove, and R. Baker, "Comparing methods of estimating the total body centre of mass in three-dimensions in normal and pathological gaits," *Human Movement Sci.*, vol. 18, no. 5, pp. 637–646, Oct. 1999.

[13] E. M. Gutierrez-Farewik, Å. Bartonek, and H. Saraste, "Comparison and evaluation of two common methods to measure center of mass displacement in three dimensions during gait," *Hum. Movement Sci.*, vol. 25, no. 2, pp. 238–256, Apr. 2006.

[14] T. J. W. Buurke and R. Den Otter, "The relationship between the anteroposterior and mediolateral margins of stability in able-bodied human walking," *Gait Posture*, vol. 90, pp. 80–85, Oct. 2021.

[15] A. L. Hof, "The 'extrapolated center of mass' concept suggests a simple control of balance in walking," *Hum. Movement Sci.*, vol. 27, no. 1, pp. 112–125, Feb. 2008.

[16] F. Watson, P. C. Fino, M. Thornton, C. Heracleous, R. Loureiro, and J. J. H. Leong, "Use of the margin of stability to quantify stability in pathologic gait—A qualitative systematic review," *BMC Musculoskeletal Disorders*, vol. 22, no. 1, pp. 1–29, Dec. 2021.

[17] G. F. Devetak, R. C. D. Bohrer, A. L. F. Rodacki, and E. F. Manffra, "Center of mass in analysis of dynamic stability during gait following stroke: A systematic review," *Gait Posture*, vol. 72, pp. 154–166, Jul. 2019.

[18] Y. Ma, K. Mithraratne, N. Wilson, Y. Zhang, and X. Wang, "Kinect V2-based gait analysis for children with cerebral palsy: Validity and reliability of spatial margin of stability and spatiotemporal variables," *Sensors*, vol. 21, no. 6, p. 2104, Mar. 2021.

[19] W. Higgins, "A comparison of complementary and Kalman filtering," *IEEE Trans. Aerosp. Electron. Syst.*, vol. AES-11, no. 3, pp. 321–325, May 1975.

[20] P. Zarchan and H. Musoff, *Progress in Astronautics and Aeronautics: Fundamentals of Kalman Filtering: A Practical Approach*. Reston, VA, USA: American Institute of Aeronautics and Astronautics, 2013.

[21] J. Carpentier, M. Benallegue, N. Mansard, and J.-P. Laumond, "Center-of-mass estimation for a polyarticulated system in contact—A spectral approach," *IEEE Trans. Robot.*, vol. 32, no. 4, pp. 810–822, Aug. 2016.

[22] J. Carpentier, "Computational foundations of anthropomorphic locomotion," Ph.D. dissertation, Lab. Anal. Archit. Syst., Université Toulouse 3 Paul Sabatier, Toulouse, France, 2017.

[23] H. Herr and M. Popovic, "Angular momentum in human walking," *J. Exp. Biol.*, vol. 211, pp. 467–481, Feb. 2008.

[24] P. Sardain and G. Bessonnet, "Forces acting on a biped robot. Center of pressure-zero moment point," *IEEE Trans. Syst., Man, Cybern. A, Syst. Humans*, vol. 34, no. 5, pp. 630–637, Sep. 2004.

[25] *Multiple Speed Walking Simulations*. Accessed: Oct. 15, 2022. [Online]. Available: http://web.archive.org/web/20220125051354/https://simtk.org/frs/?group_id=317

[26] M. H. Schwartz, A. Rozumalski, and J. P. Trost, "The effect of walking speed on the gait of typically developing children," *J. Biomech.*, vol. 41, no. 8, pp. 1639–1650, 2008.

[27] M. Q. Liu, F. C. Anderson, M. H. Schwartz, and S. L. Delp, "Muscle contributions to support and progression over a range of walking speeds," *J. Biomech.*, vol. 41, no. 15, pp. 3243–3252, Nov. 2008.

[28] C. Malloggi et al., "Three-dimensional path of the body centre of mass during walking in children: An index of neural maturation," *Int. J. Rehabil. Res.*, vol. 42, no. 2, pp. 112–119, 2019.